

Thermal Hall effect and the Wiedemann-Franz law in Chern insulator

Anxin Wang(王安新) and Tao Qin(秦涛)
Citation: Chin. Phys. B, 2023, 32 (**10**): 107301. DOI: 10.1088/1674-1056/ace158

Journal homepage: http://cpb.iphy.ac.cn; http://iopscience.iop.org/cpb

What follows is a list of articles you may be interested in

Phase transition in bilayer quantum Hall system with opposite magnetic field

Ke Yang(杨珂)
Chin. Phys. B, 2023, 32 (**9**): 097303. DOI: 10.1088/1674-1056/ace61d

Current carrying states in the disordered quantum anomalous Hall effect

Yi-Ming Dai(戴镒明), Si-Si Wang(王思思), Yan Yu(禹言), Ji-Huan Guan(关济寰), Hui-Hui Wang(王慧慧), and Yan-Yang Zhang(张艳阳)
Chin. Phys. B, 2022, 31 (**9**): 097302. DOI: 10.1088/1674-1056/ac5d2b

Generalization of the theory of three-dimensional quantum Hall effect of Fermi arcs in Weyl semimetal

Mingqi Chang(苌名起), Yunfeng Ge(葛云凤), and Li Sheng(盛利)
Chin. Phys. B, 2022, 31 (**5**): 057304. DOI: 10.1088/1674-1056/ac5c32

Entanglement spectrum of non-Abelian anyons

Ying-Hai Wu(吴英海)
Chin. Phys. B, 2022, 31 (**3**): 037302. DOI: 10.1088/1674-1056/ac280d

Integer quantum Hall effect in Kekulé-patterned graphene

Yawar Mohammadi and Samira Bahrami
Chin. Phys. B, 2022, 31 (**1**): 017305. DOI: 10.1088/1674-1056/ac1b82

Thermal Hall effect and the Wiedemann–Franz law in Chern insulator

Anxin Wang(王安新) and Tao Qin(秦涛)†

School of Physics and Optoelectronics Engineering, Anhui University, Hefei 230601, *China*

(Received 19 March 2023; revised manuscript received 12 June 2023; accepted manuscript online 25 June 2023)

Thermal Hall effect, where a transverse temperature difference is generated by implementing a longitudinal temperature gradient and an external magnetic field in the perpendicular direction to systems, is a useful tool to reveal transport properties of quantum materials. A systematic study of the thermal Hall effect in a Chern insulator is still lacking. Here, using the Landauer–Büttiker formula, we investigated the thermal Hall transport of the Harper–Hofstadter model with flux $\varphi = 1/2$ and its generalizations. We demonstrated that the Wiedemann–Franz law, which states that the thermal Hall conductivity is linearly proportional to the quantum Hall conductivity in the low temperature limit, is still valid in this Chern insulator, and that the thermal Hall conductivity can be used to characterize the topological properties of quantum materials.

Keywords: thermal Hall effect, quantum Hall effect, Chern insulator, Landauer–Büttike formula

PACS: 73.22.–f, 73.43.–f, 73.63.–b **DOI:** 10.1088/1674-1056/ace158

1. Introduction

Topological properties of the quantum materials have been under extensive studies in the last decades. Thermal Hall effect is a versatile probe to investigate transport properties of quantum materials. The Wiedemann–Franz law states that in the low temperature limit $\kappa_{xy} = L_0\sigma_{xy}T$ with $L_0 = (\pi^2/3)(k_B/e)^2$ the Lorentz number[1] and σ_{xy} the quantum Hall conductivity. Whether the Wiedemann–Franz law is valid in quantum materials is an interesting topic. Its validity has been verified theoretically,[2] where the key ingredient for the Wiedemann–Franz law to be valid is that there is a single non-interacting carrier for charge and thermal current, and experimentally[3] for anomalous Hall insulators.[4] Possible violations of the Wiedemann–Franz law has been explored in graphene,[5] where electrons and holes contribute differently to the quantum charge and thermal Hall transport due to special band structures of graphene in the magnetic field, and quasi-one dimensional conductor,[6] where an extra contribution of spinon to the thermal current has been identified. In high-temperature superconductors, huge thermal Hall conductivity and a violation of the Wiedemann–Franz law has been demonstrated[7] because of the contribution of chiral phonon to the thermal transport in the pseudogap phase of cuprates,[8] and opened a different avenue to rich physics.

Recent experimental progress has made it possible to investigate transport properties of topological materials under effectively very strong magnetic fields. The Haldane model[9] and the Harper–Hofstadter (HH) model,[10,11] as two paradigmatic models of Chern insulators to introduce magnetic fluxes, have served as playgrounds for seminal ideas. However, for a long time, the interesting properties of materials in this scenario is elusive to be observed in laboratories because of the requirement of hugely strong magnetic fields. Recently, great breakthroughs have been achieved. The Haldane model is realized with the ultracold atoms in the shaken honeycomb optical lattices,[12,13] and the HH model is realized with Raman laser assisted tunneling in the optical lattice[14,15] and in the Moiré superlattice.[16,17] These achievements afford us the possibility to investigate Chern insulators with large fluxes.

In this work, we start with the HH model at $\varphi = 1/2$, an interesting case with two Dirac cones in the first Brillouin zone, and with its generalization to introduce the complex next-nearest neighbor (NNN) hopping as the Harper–Hofstadter–Hatsugai (HHH) model.[18] For the HH model, the merging dynamics of Dirac cones resulting from uniaxial staggered potential in the first magnetic Brillouin zone (MBZ) has been investigated.[19] By combing the Bott index[20] and on-site disorders, the topological properties enhanced by onsite disorders and interactions has been detailed studied.[21,22] However, a detailed study of thermal Hall transport of the HHH model is still lacking. Using the Landauer–Büttiker formula,[5,23] we systematically investigate the quantum charge/thermal Hall transport in the HHH model with uniaxial staggered potentials presented, identify the validity of the Wiedemann–Franz law, and show that it is possible to characterize topological properties by the thermal Hall conductivity. Moreover, we introduce a small perturbation to the flux with $\varphi = 1/2 + \delta\varphi$,[19,24] equivalent to an effective magnetic field on top of the flux $\varphi = 1/2$, which brings about interesting transport physics. We need to point out that the defining property for the Chern insulator is the non-zero Chern invariant related to occupied Bloch bands, quite extensively discussed in the Haldane model,[25] and that the HHH model with a

†Corresponding author. E-mail: taoqin@ahu.edu.cn

© 2023 Chinese Physical Society and IOP Publishing Ltd

perturbation in the flux is still a Chern insulator because of non-trivial topological properties for occupied Bloch bands. Our work offers a different point of view to reveal topological properties of quantum materials.

The remainder of the paper is organized as follows. In Section 2, we presented our model and methods. In Section 3, we show our results on the quantum charge/thermal Hall conductivity for three typical cases, and its possibility to be realized in experiments is also discussed. In Section 4, a short summary and outlook is given. Because of a pedagogical purpose, we present some technique details in the Appendix A.

2. Model and methods

Firstly, we introduce the HHH model with uni-axial staggered potential on a two-dimensional square lattice,

$$\begin{aligned} H = \sum_{m,n} \big[& -t_{\mathrm{a}} c^{\dagger}_{m,n+1} c_{m,n} - t_{\mathrm{b}} \mathrm{e}^{-\mathrm{i}2\pi\varphi n} c^{\dagger}_{m+1,n} c_{m,n} \\ & - t_{\mathrm{c}} \mathrm{e}^{-\mathrm{i}2\pi\varphi(n+1/2)} c^{\dagger}_{m+1,n+1} c_{m,n} \\ & - t'_{\mathrm{c}} \mathrm{e}^{\mathrm{i}2\pi\varphi(n+1/2)} c^{\dagger}_{m,n+1} c_{m+1,n} \\ & + \Delta (-1)^n c^{\dagger}_{m,n} c_{m,n} + \mathrm{h.c.} \big], \end{aligned} \tag{1}$$

where m, n labels x and y coordinates of the sites. We consider a commensurate flux $\varphi = 1/2$. Δ is the strength for the uniaxial staggered potential. Different from the usual HH model, the HHH model is featured in the NNN hopping with a complex phase. The staggered potential Δ breaks the inversion symmetry, but keeps the reflection symmetry in the x direction, therefore, a moderate strength of Δ shift positions of degenerate points, and strong enough one would open a gap. When $t_{\mathrm{c}} \neq t'_{\mathrm{c}}$, it breaks all symmetry operations in symmetry group C_4, so a non-zero t_{c} or t'_{c} would open a gap immediately. In this work, we focus on how to tune the topological properties with changes in parameters such as t_{c}, t'_{c}, φ, and Δ.

Following the method in Refs. [18,19], we briefly outline how to obtain the quantum Hall conductivity of the HHH model at $\varphi = 1/2$ with the uniaxial staggered potentials. Setting $n = ql + j$ with l the cell index, $q = 2$, and $j = 1, 2, \ldots, q$, and using the Fourier transformation

$$c_{mn} = c_{j,l,n} = \frac{1}{(2\pi)^2} \int_{-\pi}^{\pi} \mathrm{d}k_x \int_{-\pi/q}^{\pi/q} \mathrm{d}k_y \, \mathrm{e}^{\mathrm{i}\left(k_x m + q k_y l\right)} c_{j,\boldsymbol{k}},$$

we have

$$H = \frac{1}{(2\pi)^2} \int_{-\pi}^{\pi} \mathrm{d}k_x \int_{-\pi/q}^{\pi/q} \mathrm{d}k_y H_{\boldsymbol{k}}, \tag{2}$$

$$H_{\boldsymbol{k}} = \sum_{j=1}^{q} A_{j\boldsymbol{k}} c^{\dagger}_{j,\boldsymbol{k}} c^{\dagger}_{j,\boldsymbol{k}} + B_{j\boldsymbol{k}} c^{\dagger}_{j,\boldsymbol{k}} c_{j+1,\boldsymbol{k}} + \mathrm{h.c.}, \tag{3}$$

where $A_{j\boldsymbol{k}} = -2t_{\mathrm{b}} \cos\left(k_x + 2\pi\varphi j\right) + \Delta(-1)^j$, $B_{j\boldsymbol{k}} = -t_{\mathrm{a}} - t_{\mathrm{c}} \mathrm{e}^{-\mathrm{i}2\pi\varphi(j+1/2) - \mathrm{i}k_x} - t'_{\mathrm{c}} \mathrm{e}^{\mathrm{i}2\pi\varphi(j+1/2) + \mathrm{i}k_x}$, and $c_{j+1,\boldsymbol{k}} = c_{k_x, k_y + 2\pi j\varphi}$, with the boundary condition $c_{q+1,\boldsymbol{k}} = c_{q,\boldsymbol{k}} \mathrm{e}^{\mathrm{i}qk_y}$. We have set the lattice constant $a = 1$. For $q = 2$, we can write $H_{\boldsymbol{k}} = \left(c^{\dagger}_{1\boldsymbol{k}} \;\; c^{\dagger}_{2\boldsymbol{k}} \right) \tilde{H}_{\boldsymbol{k}} \left(c_{1\boldsymbol{k}} \;\; c_{2\boldsymbol{k}} \right)^{\mathrm{T}}$ and

$$\tilde{H}_{\boldsymbol{k}} = \begin{pmatrix} A_{\boldsymbol{k}} & B_{\boldsymbol{k}} \\ B^*_{\boldsymbol{k}} & -A_{\boldsymbol{k}} \end{pmatrix}, \tag{4}$$

where $A_{\boldsymbol{k}} = 2t_{\mathrm{b}} \cos k_x - \Delta$, and $B_{\boldsymbol{k}} = B_{1\boldsymbol{k}} + B^*_{2\boldsymbol{k}} \mathrm{e}^{-2\mathrm{i}k_y} = -2\mathrm{e}^{-\mathrm{i}k_y} \left(t_{\mathrm{a}} \cos k_y + \mathrm{i}t_{\mathrm{c}} \cos\left(k_x - k_y\right) - \mathrm{i}t'_{\mathrm{c}} \cos\left(k_x + k_y\right) \right)$.

A few remarks on the Hamiltonian in Eq. (4) for $\varphi = 1/2$ are in order. (i) When $t_{\mathrm{c}} = t'_{\mathrm{c}} = \Delta = 0$, there are two Dirac points locating at $\boldsymbol{k} = (\pm\pi/2, \pi/2)$; (ii) When $\Delta = 0$ and $t_{\mathrm{c}} + t'_{\mathrm{c}} = 0$, the two Dirac points at $\boldsymbol{k} = (\pm\pi/2, \pi/2)$ can be preserved; (iii) Non-zero uniaxial staggered potential would result in the merging of Dirac points.[19]

We then have a brief review of methods to calculate the quantum Hall conductivity and thermal Hall conductivity. Following the method of Ref. [18] Appendix A1, we have shown that the quantum Hall conductivity of the electron for the half-filling case is

$$\sigma_{xy} = \frac{\mathrm{e}^2}{h} \mathrm{sgn}\left(t_{\mathrm{a}} \left(t_{\mathrm{c}} + t'_{\mathrm{c}} \right) \right), \tag{5}$$

with the condition that $t_{\mathrm{b}} > 0$, $t_{\mathrm{a}} \neq 0$, $t_{\mathrm{c}} + t'_{\mathrm{c}} \neq 0$, and $|\Delta| < 2t_{\mathrm{b}}$. Electrons, as charge carriers, can transport energy simultaneously, and lead to the thermal Hall effect. One can show that for this model the Wiedemann–Franz law is valid at the low temperature limit.[2,26] All these derivations are based on bulk formulas.

In this work we focus on the quantum charge and thermal Hall transport in a nano-structure based on the Landauer–Büttiker formula,[5,23,27,28] explore the validity of the Wiedemann–Franz law, and demonstrate that the non-trivial topological properties can be revealed by the thermal Hall conductivity. As shown in Fig. 1, the nano-structure consists of a central system described by the Hamiltonian in Eq. (1) and six simple leads. The charge current flowing to the terminal n can be described by the Landauer–Büttiker formula as

$$I_n = \frac{\mathrm{e}^2}{h} \sum_{m(\neq n)=1}^{6} \int T_{nm}(E) \left(f_n(E) - f_m(E) \right) \mathrm{d}E, \tag{6}$$

where the transmission coefficient from terminal n to m is $T_{nm}(E) = \mathrm{Tr}\left[\Gamma_n G^{\mathrm{R}} \Gamma_m G^{\mathrm{A}} \right]$. $f_n(E) = 1/\left[\mathrm{e}^{(E - V_n)/(k_{\mathrm{B}} T)} + 1 \right]$ is the Fermi–Dirac distribution function with V_n the voltage for terminal n. The line width function $\Gamma_n(E) = \mathrm{i}\left(\Sigma^{\mathrm{R}}_n(E) - \Sigma^{\mathrm{A}}_n(E) \right)$ with the self-energy Σ^{R}_n resulted from coupling the system to the lead n and $\Sigma^{\mathrm{R}}_n = \left(\Sigma^{\mathrm{A}}_n \right)^{\dagger}$. The retarded Green's function $G^{\mathrm{R}}(E) = \left(G^{\mathrm{A}} \right)^{\dagger} = \left[EI - H_{\mathrm{c}} - \sum_{n=1}^{6} \Sigma_n \right]^{-1}$ with I the identity matrix and H_{c} the Hamiltonian for the central region (blue part in Fig. 1). To measure the quantum charge Hall conductivity, a bias voltage is applied across the terminal 1 and 4 as $V_1 = -V_4 = V/2$. In the low temperature region, $f_n(E)$ can be expanded to

the first order of the voltage. With the boundary condition as $I_2 = I_3 = I_5 = I_6 = 0$, one can obtain V_n $(n = 2,3,5,6)$. Essentially it is problem to solve inhomogeneous linear equations for V_n. As a result of current conservation, $I_1 = -I_4$. The Hall resistance and longitudinal resistance can be calculated as $R_{xy} = (V_2 - V_6)/I_1$ and $R_{xx} = (V_2 - V_3)/I_1$, respectively. Finally, the quantum Hall conductivity is defined as $\sigma_{xy} = R_{xy}/\left(R_{xy}^2 + R_{xx}^2\right)$. The quantum thermal Hall effect can be explored in a similar scenario and one is referred to Appendix A2 and Ref. [5] for details. We choose $t_a = t_b = 1$ as the energy unit.

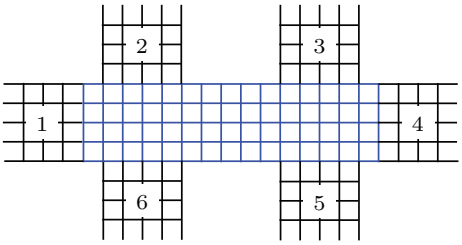


Fig. 1. A typical set-up for quantum thermal Hall and charge Hall conductivity measurement: six-terminal nano-structure consisting of system and six leads. The central region has $N+2+2L$ columns of lattice sites with $L = 5$ and $N = 4$.

3. Results and discussion

In this section, we presented our results for three different typical cases in the low temperature $T = 0.001$. Case (i): $\varphi = 1/2$ and $t_c = t_c' = 0.3$. As shown in Fig. 2, we find quantum Hall plateau for different stagger potentials in Figs. 2(a) and 2(c) in the low temperature limit. The width of the plateaus is consistent with the bulk gaps in Figs. 2(b) and 2(d), indicating that the charge transport is carried by the chiral edge states, which is a manifestation of the bulk–edge correspondence.[29,30] When $\Delta \geq 2$, the gap is closed and the plateau would disappear (Figs. 2(e) and 2(f)). In Figs. 2(a) and 2(b) one can determine the quantum Hall conductivity by counting how many edge states have been cut by the Fermi energy in Fig. 2(b), where the band structure on a cylinder periodic in the x direction is shown. The real-space distribution of different states in the y direction is encoded by color in Figs. 2(b) and 2(d), where the color value 0, and 1 indicate two ends of the cylinder. Therefore, the edge states can be clearly identified. The numerical results for the quantum Hall conductivity is also the same as predicted by the analytical formula in Eq. (5), and the consistence benchmarked our working codes. We recall that the Harper–Hofstadter model at $\varphi = 1/2$ with $\Delta = 0$ is semi-metallic.[19] It demonstrates that the topological properties of this model can be tuned by introduction of the complex next-nearest neighbor hopping. The quantum thermal Hall conductivity κ_{xy} normalized by $\pi^2 k_B^2 T/3h$ is nearly in coincident with σ_{xy} as $\kappa_{xy} = L_0 \sigma_{xy}$, indicating that the Wiedemann–Franz law is valid in the low temperature limit. Moreover, it means that one can reveal topological properties of a system by exploring the thermal Hall effect.

We need to point out the a couple of issues in the numerical results. (i) It is about the numerical stability beyond the plateau in Figs. 2(a), 2(c), and 2(e), where very steep lines show up. In this energy region, the bulk is metallic. The apparent imperfect agreement between the two quantities in the metallic phase results from two main factors. Firstly, it is the physics reason. We carried our calculations at $T = 0.001$ with the NN hopping as the energy unit, and the Wiedemann–Franz law is valid in the low temperature limit. While the finite temperature effect can be forbidden by large energy gap in the Chern insulator phase, it shows up when the system is in the metallic phase. We next turn to the technical reasons. The key part of our numerical calculations is to solve inhomogeneous linear equations. Indeed, in metallic phase the numerical stability is not perfect for some parameters, as introduces relatively large deviations between charge and thermal Hall conductivities. We tried different ways to solve linear equations and the method of least squares, which we implemented in the codes, turned out to be a better one. (ii) In Fig. 2(d), there is clearly discontinuity in the color of the bands around $k_x = 2$, and it is a reflection of the fixed boundary condition in the y direction of the cylinder.

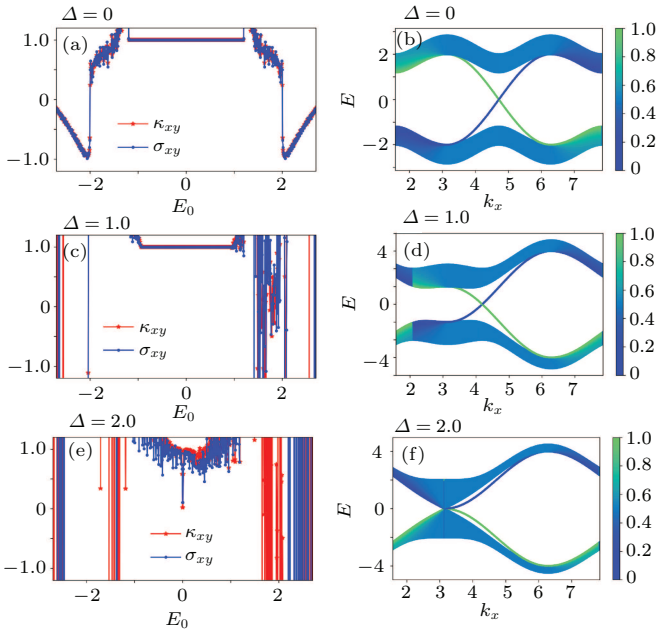


Fig. 2. Panels (a), (c), and (e) are the quantum thermal Hall conductivity κ_{xy} (normalized by $\pi^2 k_B^2 T/3h$) and charge Hall conductivity σ_{xy} (normalized by e^2/h) versus the Fermi energy E for different staggered potential Δ, and their corresponding band structure with color encoded y position versus k_x on a cylinder structure with periodic boundary condition in the x direction and open boundary condition in the y direction with a width of 400 in panels (b), (d), and (f). Other parameters are $t_a = t_b = 1$, $t_c = t_c' = 0.3$, and $\varphi = 1/2$. The temperature $T = 0.001$, which is very low compared with typical gaps around $E = 0$. The size of the six-terminal structure in numerical calculations is $N = L = 80$.

Case (ii): $\varphi = 1/2 + \delta\varphi$, $\delta\varphi = 0.05$, and $t_c = t_c' = 0$. We go beyond the canonical case of $\varphi = 1/2$ and introduce a

small perturbation to the integer flux.[19,24] It is equivalent to a small effective magnetic flux $\delta\varphi = 0.05$ on top of $\varphi = 1/2$. Similar to results for case (i) in Fig. 2, we find the same coincidence between the quantum Hall conductivity σ_{xy} and thermal Hall conductivity κ_{xy} in Fig. 3, indicating the validity of the Wiedemann–Franz law. Furthermore, we would like to point out that the picture of chiral edge states still works for this case.

One new feature for case (ii) is the steep change of the charge/thermal Hall conductivity around the Fermi energy $E_0 = 0$ (Figs. 3(a) and 3(c)). It is due to the change in the direction of the chiral edge states. We take Fig. 3(b) as an example. The edge state with positive velocity (green lines) in the gap just below $E_0 = 0$, change its direction in the gap just above $E_0 = 0$. It is this motion direction reversal which brings about the sign change in the charge/thermal Hall conductivity around $E_0 = 0$, because carriers tansport both charge and energy. Therefore, as we have claimed, the Wiedemann—Franz is still valid for this case. Furthermore, we need to point out that one can generally characterize the topological properties of a system with thermal Hall conductivity.

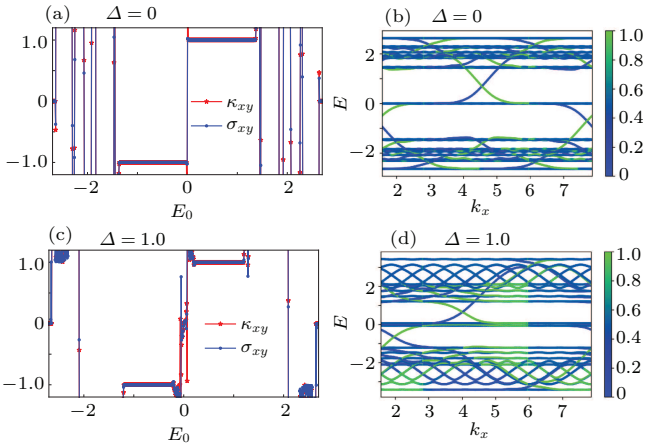


Fig. 3. The physical quantities shown are the same as those in Fig. 2. Different parameters are $t_c = t_c' = 0$, $\varphi = 1/2 + \delta\varphi$, and $\delta\varphi = 0.05$.

For case (ii), $\varphi = 11/20$, so we find there are 20 energy bands in Fig. 3(b) and 3(d), where some bands are nearly flat, a reflection of the Landau level. A zoom-in shown in Figs. 4(a) and 4(b), corresponding to Figs. 3(b) and 3(d) respectively, preseents the fine structures of the nearly flat bands. Moreover, we show the density of states (DOS) of the bulk bands in Fig. 4, where we find that peaks show up for every bulk bands.

Case (iii): $\varphi = 1/2 + \delta\varphi$, $\delta\varphi = 0.05$, and $t_c = t_c' = 0.3$. In Figs. 5(a) and 5(c), we find the same steep change in the charge/thermal Hall conductivity, which can be explained by the direction change in the edge states. In this case we have introduced the NNN hopping, and it indicates that this kind of steep changes in conductivity are rather universal. Even though there is anisotropy brought about by the NNN hopping, the Wiedemann–Franz law is still valid.

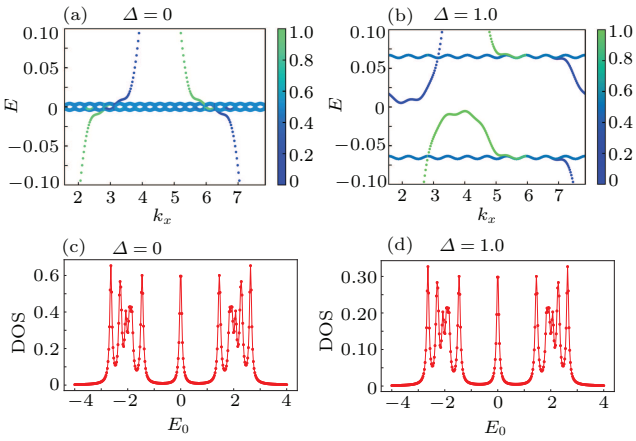


Fig. 4. Panels (a) and (b) are zoom-in of the band structures of Figs. 3(b) and 3(d) around $E = 0$, respectively. Panels (c) and (d) are density of states (DOS) for case (ii). DOS is obtained numerically with a Lorentzian function $\mathrm{DOS}(E) = \frac{1}{\pi}\lim_{\varepsilon\to 0^+}\sum_{k_x\in \mathrm{BZ}} \frac{\varepsilon}{(E-E_{k_x})^2+\varepsilon^2}$, where BZ stands for the first Brillouin zone. The line-width parameter $\varepsilon = 0.05$ in the calculations. To remove the effects of edge states we also implement periodic boundary condition in the x direction. We highlight the sharp peaks around $E = 0$ in DOS which corresponds to the bulk bands.

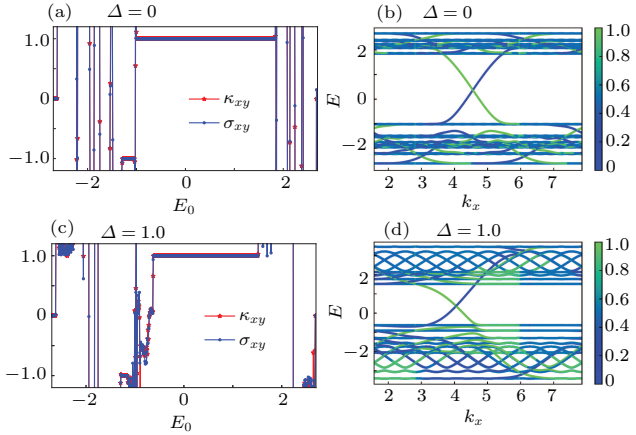


Fig. 5. The physical quantities shown are the same as those in Fig. 2, but with parameters as $t_c = t_c' = 0.3$, $\varphi = 1/2 + \delta\varphi$, and $\delta\varphi = 0.05$.

We finally discuss the possible experimental realization. In a real material, the NNN hopping amplitudes t_c, and t_c' can be tuned by strain[31] and laser irradiation.[32] Onsite staggered potential Δ is usually induced by substrates. The flux φ can certainly be adjusted by strength of external magnetic fields.

Our numerical simulation involves an extremely strong magnetic field. We have an estimate of the strength of magnetic fields required to realize the $1/2$ flux by $Bl^2 = (p/q)(h/e)$ where the lattice constant l is approximately 1 Å and $p/q = 1/2$. It follows that $B \approx 4 \times 10^4$ T, far beyond the reach in the laboratory, where the world record for strongest steady magnetic field is as high as approximately 45.22 T achieved on August 12 2023, in Hefei China, which cannot be directly achieved in the laboratory. However, indirectly,

one can realize it with the help of the moiré superlattice,[16,17] topolectrical circuits,[33] or Raman laser assisted tunneling of ultracold atoms in the optical lattice.[14,15] So far all the three techniques are rather sophisticated. We also need to point out that the HHH model has been realized in the metamaterial of topoelectrical circuits.[34] The possible proposal for experiment realizations in real materials will be explored in the near future.

4. Summary and outlook

To sum up, we have investigated the quantum charge/thermal Hall effect in the HH model and its generalization. We have numerically studied the quantum charge/thermal Hall conductivity in a six-terminal nanostructure and understood it from the point of view of the bulk-edge correspondence. We demonstrate that the Wiedemann–Franz law is valid in the Chern insulator, even though there is a steep change of the Hall conductivity around $E_0 = 0$. Our calculations show that the non-trivial topological properties can be revealed by both the charge Hall conductivity and the thermal Hall conductivity.

Appendix A: Energy spectrum of a cylinder structure

To make the results in this work self-contained, we present some details in this section following the methods outlined in Refs. [5,18,23].

Appendix A1: Quantum Hall conductivity of the HHH model with staggered potential

Following the method in Ref. [18], we presented the derivation of the quantum Hall conductivity of the HHH model at $\varphi = 1/2$ with a staggered potential. We choose the first MBZ as $k_x \in [-\pi, \pi]$ and $k_y \in [0, \pi]$. The Hamiltonian in Eq. (4) reads

$$\tilde{H}_{\boldsymbol{k}} = \sqrt{A_{\boldsymbol{k}}^2 + B_{\boldsymbol{k}}^2} \begin{pmatrix} \cos(2\theta) & \sin(2\theta)\, \mathrm{e}^{\mathrm{i}\zeta_{\boldsymbol{k}}} \\ \sin(2\theta)\, \mathrm{e}^{-\mathrm{i}\zeta_{\boldsymbol{k}}} & -\cos(2\theta) \end{pmatrix}, \quad \text{(A1)}$$

where $\cos(2\theta) = \frac{A_{\boldsymbol{k}}}{\sqrt{A_{\boldsymbol{k}}^2+B_{\boldsymbol{k}}^2}}$, $\sin(2\theta) = \frac{|B_{\boldsymbol{k}}|}{\sqrt{A_{\boldsymbol{k}}^2+B_{\boldsymbol{k}}^2}}$, and $B_{\boldsymbol{k}} = |B_{\boldsymbol{k}}|\, \mathrm{e}^{\mathrm{i}\zeta_{\boldsymbol{k}}}$. The eigenvalues of $\tilde{H}_{\boldsymbol{k}}$ are

$$\begin{aligned} E_{\pm}(\boldsymbol{k}) = & \pm 2t_{\mathrm{b}}((\cos k_x - \Delta/(2t_{\mathrm{b}}))^2 \\ & + (t_{\mathrm{a}}/t_{\mathrm{b}})^2 \cos^2 k_y + (t_{\mathrm{c}}/t_{\mathrm{b}})^2 \cos^2(k_x - k_y) \\ & + (t_{\mathrm{c}}'/t_{\mathrm{b}})^2 \cos^2(k_x + k_y))^{1/2}. \end{aligned}$$

The eigenvector for the lower band is

$$(a, b)^{\mathrm{T}} = \left(-\sin\theta, \cos\theta\, \mathrm{e}^{-\mathrm{i}\zeta_{\boldsymbol{k}}}\right)^{\mathrm{T}},$$

where we have chosen a gauge with the component a as real and set $b = \tilde{b}\, \mathrm{e}^{-\mathrm{i}\zeta_{\boldsymbol{k}}}$. The quantum Hall conductivity for the lower band can be calculated as[18,35]

$$\sigma_{xy} = \frac{e^2}{h} \frac{1}{2\pi\mathrm{i}} \sum_{\Delta_i} \oint_{\Delta_i} \mathrm{d}\boldsymbol{k} \cdot (a^*, b^*) \nabla_{\boldsymbol{k}} \begin{pmatrix} a \\ b \end{pmatrix},$$

where Δ_i refers to different parts for the first MBZ. Because a is real,

$$\sigma_{xy} = \frac{e^2}{h} \frac{1}{2\pi\mathrm{i}} \sum_{\Delta_i} \oint_{\Delta_i} \mathrm{d}\boldsymbol{k} \cdot \left(-\mathrm{i}\tilde{b}^2 \nabla_{\boldsymbol{k}} \zeta_{\boldsymbol{k}}\right).$$

As shown in Fig. A1, only three paths contribute to the integral. Because around path II, $\tilde{b}^2 = 0$, the contribution from path II vanishes. On path I, $\tilde{b}^2 = 1/2$, we have $k_{x0} = \arccos \Delta/2t_{\mathrm{b}}$ with the assumption that $|\Delta| < 2t_{\mathrm{b}}$, $B_{\boldsymbol{k}} = -2\mathrm{e}^{-\mathrm{i}k_y}(t_{\mathrm{a}} \cos k_y + \mathrm{i}\,(t_{\mathrm{c}} - t_{\mathrm{c}}') \cos k_{x0} \cos k_y - \mathrm{i}\,(t_{\mathrm{c}} + t_{\mathrm{c}}') \sin k_{x0} \sin k_y)$. When k_y varies from 0 to π, the two factors in $B_{\boldsymbol{k}}$ will contribute a 2π change in the phase, thus we obtain $\oint_{\mathrm{I}} \mathrm{d}\boldsymbol{k} \cdot \left(-\mathrm{i}\tilde{b}^2 \nabla_{\boldsymbol{k}} \zeta_{\boldsymbol{k}}\right) = -2\pi \mathrm{sgn}(t_{\mathrm{a}}(t_{\mathrm{c}} + t_{\mathrm{c}}'))$. For path II, we have similar result. In total, we come to the final form in Eq. (5).

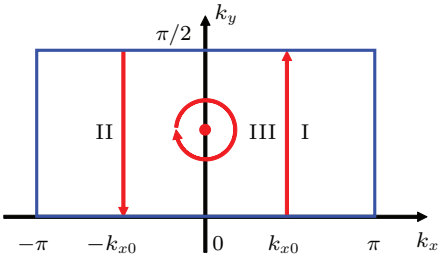


Fig. A1. Integral paths indicated by red lines for the derivation of the quantum Hall conductivity. $k_{x_0} = \arccos \Delta/2t_{\mathrm{b}}$.

Appendix A2: Thermal Hall conductivity calculation based on the Landauer–Büttiker formula

We adopt the method in Refs. [5,23,27,28] to calculate the thermal Hall conductivity. We firstly expand respectively the charge current

$$I_n = \sum_m \int \mathrm{d}E T_{nm}(E)\,[f_n(E) - f_m(E)]$$

and energy current $J_n = \sum_m \int \mathrm{d}E\,(E - V_n)\, T_{nm}\,[f_n(E) - f_m(E)]$ to the first order of voltage V_n and temperature T_n ($n = 1, 2, \ldots, 6$) as follows:

$$I_n \approx \sum_{m(\neq n)=1}^{6} -P_{nm}(V_n - V_m) + Q_{nm}(T_n - T_m), \quad \text{(A2)}$$

$$\begin{aligned} J_n \approx & \sum_{m(\neq n)=1}^{6} \int \mathrm{d}E T_{nm}[-(V_n - V_m) E \partial_E f_0 \\ & + (T_n - T_m) E \partial_T f_0], \end{aligned} \quad \text{(A3)}$$

where we have defined $P_{nm} = \int \mathrm{d}E T_{nm}(E)\, \partial_E f_0$, $Q_{nm} = \int \mathrm{d}E T_{nm}(E)\, \partial_T f_0$, $R_{nm} = \int \mathrm{d}E E T_{nm}(E)\, \partial_E f_0$, and $S_{nm} = \int \mathrm{d}E E T_{nm}(E)\, \partial_T f_0$. For all these newly defined quantities,

$n \neq m$. We have a short comment on the integration. Since the temperature is rather low, the integral interval can be limited to a few $k_B T$ around the Fermi energy. To obtain the thermal Hall effect, a temperature gradient is applied across terminal 1 and 4, and we set $J_n = 0$ $(n = 2,3,5,6)$ and $I_n = 0$, $(n = 1,2,\ldots,6)$. Due to thermal current conservation, $J_1 = -J_4$. Therefore, we obtain a group of linear inhomogeneous equations for unknown quantities T_n, $(n = 2,3,5,6)$ and $V_n = 0$, $(n = 1,2,\ldots,6)$ as follows:

$$I_n = \sum_{m=1}^{6} P_{nm} V_m - Q_{nm} T_m, \tag{A4}$$

$$J_{n'} = \sum_{m=1}^{6} R_{n'm} V_m - S_{n'm} T_m, \tag{A5}$$

where $n = 2,3,5,6$, and $n' = 1,2,\ldots,6$. Note in Eqs. (A4) and (A5), we have redefined $P_{11} = -\sum_{n\neq 1} P_{1n}$, and similarly for Q_{11}, R_{11}, and S_{11}. To solve the linear equations, a method of least square solutions is important to obtain a stable solution. The thermal Hall resistance and longitudinal resistance can be calculated as $\tilde{R}_{xy} = (J_2 - J_6)/T_1$ and $\tilde{R}_{xx} = (J_2 - J_3)/T_1$, respectively. Finally, the quantum thermal Hall conductivity is defined as $\kappa_{xy} = \tilde{R}_{xy}/\left(\tilde{R}_{xy}^2 + \tilde{R}_{xx}^2\right)$.

Acknowledgements

Project supported by the National Natural Science Foundation of China (Grant Nos. U2032164 and 12174394) and the Start-up Fund from Anhui University in China.

References

[1] Kane C L and Fisher M P A 2005 *Phys. Rev. B* **55** 15832
[2] Qin T, Niu Q and Shi J 2011 *Phys. Rev. Lett.* **107** 236601
[3] Onose Y, Shiomi Y and Tokura Y 2008 *Phys. Rev. Lett.* **100** 016601
[4] Nagaosa N, Sinova J, Onoda S, MacDonald A H and Ong N P 2010 *Rev. Mod. Phys.* **82** 1539
[5] Long W, Zhang H and Sun Q F 2011 *Phys. Rev. B* **84** 075416
[6] Wakeham N, Bangura A F, Xu X, Mercure J F, Greenblatt M and Hussey N E 2011 *Nat. Commun.* **2** 396
[7] Grissonnanche G, Legros A, Badoux S, Lefrançois E, Zatko V, Lizaire M, Laliberté F, Gourgout A, Zhou J S, Pyon S, *et al.* 2019 *Nature* **571** 376
[8] Grissonnanche G, Thériault S, Gourgout A, Boulanger M E, Lefrançois E, Ataei A, Laliberté F, Dion M, Zhou J S, Pyon S, *et al.* 2020 *Nat. Phys.* **16** 1108
[9] Haldane F D M 1988 *Phys. Rev. Lett.* **61** 2015
[10] Harper P G 1955 *Proc. Phys. Soc. A* **68** 874
[11] Hofstadter D R 1976 *Phys. Rev. B* **14** 2239
[12] Jotzu G, Messer M, Desbuquois R, Lebrat M, Uehlinger T, Greif D and Esslinger T 2014 *Nature* **515** 237
[13] Fläschner N, Rem B S, Tarnowski M, Vogel D, Lühmann D S, Sengstock K and Weitenberg C 2016 *Science* **352** 1091
[14] Miyake H, Siviloglou G A, Kennedy C J, Burton W C and Ketterle W 2013 *Phys. Rev. Lett.* **111** 185302
[15] Aidelsburger M, Atala M, Lohse M, Barreiro J T, Paredes B and Bloch I 2013 *Phys. Rev. Lett.* **111** 185301
[16] Dean C R, Wang L, Maher P, Forsythe C, Ghahari F, Gao Y, Katoch J, Ishigami M, Moon P, Koshino M, *et al.* 2013 *Nature* **497** 598
[17] Hunt B, Sanchez-Yamagishi J D, Young A F, Yankowitz M, LeRoy B J, Watanabe K, Taniguchi T, Moon P, Koshino M, Jarillo-Herrero P, *et al.* 2013 *Science* **340** 1427
[18] Hatsugai Y and Kohmoto M 1990 *Phys. Rev. B* **42** 8282
[19] Delplace P and Montambaux G 2010 *Phys. Rev. B* **82** 035438
[20] Loring T A and Hastings M B 2010 *Europhys. Lett.* **92** 67004
[21] Kuno Y 2019 *Phys. Rev. B* **100** 054108
[22] Zheng J H, Qin T and Hofstetter W 2019 *Phys. Rev. B* **99** 125138
[23] Chen J C, Wang J and Sun Q F 2012 *Phys. Rev. B* **85** 125401
[24] Harper F, Simon S H and Roy R 2014 *Phys. Rev. B* **90** 075104
[25] Thonhauser T and Vanderbilt D 2006 *Phys. Rev. B* **74** 235111
[26] Smrcka L and Streda P 1977 *J. Phys. C: Solid State Physics* **10** 2153
[27] Cheng S G, Xing Y, Sun Q F and Xie X C 2008 *Phys. Rev. B* **78** 045302
[28] Jiang H, Cheng S, Sun Q F and Xie X C 2009 *Phys. Rev. Lett.* **103** 036803
[29] Hasan M Z and Kane C L 2010 *Rev. Mod. Phys.* **82** 3045
[30] Qi X L and Zhang S C 2011 *Rev. Mod. Phys.* **83** 1057
[31] Chauwin M, Siu Z B and Jalil M B A 2022 *Phys. Rev. Appl.* **17** 024035
[32] Oka T and Aoki H 2009 *Phys. Rev. B* **79** 081406
[33] Lee C H, Imhof S, Berger C, Bayer F, Brehm J, Molenkamp L W, Kiessling T and Thomale R 2018 *Commun. Phys.* **1** 39
[34] Yatsugi K, Yoshida T, Mizoguchi T, Kuno Y, Iizuka H, Tadokoro Y and Hatsugai Y 2022 *Commun. Phys.* **5** 180
[35] Thouless D J, Kohmoto M, Nightingale M P and den Nijs M 1982 *Phys. Rev. Lett.* **49** 405